Journal of Power Sources 263 (2014) 310–314

Contents lists available at ScienceDirect

Journal of Power Sources

journal homepage: www.elsevier.com/locate/jpowsour

Short communication

Nickel-doped ceria nanoparticles for promoting catalytic activity of Pt/C for ethanol electrooxidation

Qiang Tan, Chunyu Du*, Yongrong Sun, Lei Du, Geping Yin, Yunzhi Gao

School of Chemical Engineering & Technology, Harbin Institute of Technology, Harbin 150001, China

HIGHLIGHTS

- Ni-doped CeO_2 nanoparticles were synthesized by a thermal decomposition method.
- Ni-doped CeO_2 nanoparticles enhance the activity of Pt/C for ethanol electrooxidation.
- Oxygen releasing capacity and interaction with Pt of Ni-doped CeO_2 contribute to the activity.

GRAPHICAL ABSTRACT

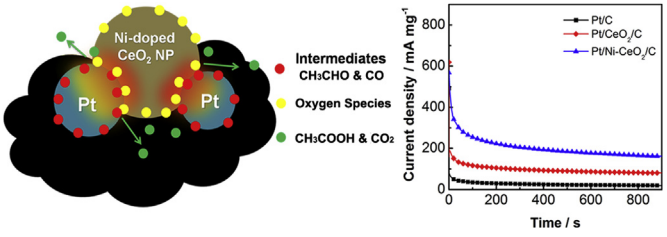

ARTICLE INFO

Article history:
Received 11 December 2013
Received in revised form
30 March 2014
Accepted 14 April 2014
Available online 24 April 2014

Keywords:
Fuel cell
Nickel-doped ceria
Electrocatalysis
Ethanol oxidation

ABSTRACT

This paper reports the facile synthesis of monodispersed nickel-doped ceria nanoparticles by a thermal decomposition method, which is used to promote catalytic properties of Pt/C. The Pt/Ni-doped CeO_2/C catalyst obtained exhibits remarkably high activity and stability towards the ethanol electrooxidation in acidic media. This is attributed to higher oxygen releasing capacity and stronger interaction of Ni-doped CeO_2 with Pt than pure CeO_2 nanoparticles that contribute positively to the removal of poisoning intermediates. We believe that the design concept and synthetic strategy of metal doped oxides used for fuel cell catalysts can be potentially extended to other catalytic fields.

1. Introduction

Direct ethanol fuel cells (DEFCs) are currently under intensive investigation for a wide range applications in transportation, stationary and portable power sources, due to their high energy density, easy fuel storage, low toxicity and high efficiency [1]. However, the quest for high loading of precious metals due to the sluggish ethanol electrooxidation poses a challenge for their development [2]. Metal oxides have been employed as the promoter of catalytic properties due to their facile oxygen-species releasing ability and well corrosion–resistance property [3]. In previous studies, various metal oxides, such as MgO [4], SiO_2 [5], MnO_2 [6], and WO_3 [7] have been explored to promote the ethanol electrooxidation kinetics, which depends highly on their interaction with precious metal electrocatalysts. Up to now, however, it still remains a challenge to further improve the interaction between metal catalysts and oxides and thus the catalytic properties, although promising results have been obtained [8].

Herein, we report the preparation of a sphere-like monodispersed Ni-doped CeO_2 (Ni–CeO_2) nanoparticles (NPs) by a facile thermal decomposition method. These Ni–CeO_2 NPs are used to promote the catalytic properties of the Pt/C catalyst in DEFCs for the first time. Compared with the conventional Pt/C and Pt/CeO_2/C catalysts, our Pt/Ni–CeO_2/C catalyst exhibits remarkably enhanced electrocatalytic activity and stability for the ethanol electrooxidation reaction in acidic media. It is revealed that the high

* Corresponding author. Tel.: +86 451 86403961; fax: +86 451 86418616.
E-mail address: cydu@hit.edu.cn (C. Du).

http://dx.doi.org/10.1016/j.jpowsour.2014.04.062
0378-7753/

content of Ce^{3+} and enhanced interaction between Pt and CeO_2 in Pt/Ni–CeO_2/C catalyst, which result from the Ni ion doping into CeO_2, are responsible for the bursts of catalytic properties. Thus, our Pt/Ni–CeO_2/C catalyst is different from the conventional PtNi/CeO_2/C catalyst, in which the contribution of Ni to activity comes from the direct interaction between Pt and metallic Ni. Our strategy provides an alternative promising approach to enhancing the activity of Pt-based fuel cell catalysts through modulating the properties of co-catalytic metal oxides.

2. Experimental

2.1. Synthesis

2.1.1. Synthesis of Ni–CeO_2 NPs

In the thermal decomposition synthesis of Ni-doped CeO_2 (Ni–CeO_2) NPs, 0.5 mmol cerium (IV) ammonium nitrate ($H_8CeN_8O_{18}$), 0.025 mmol bis(2,4-pentanediono)nickel ($C_{10}H_{14}NiO_4$), 2.46 mL oleylamine, and 10 mL 1-octadecene were homogeneously mixed by magnetic stirring under N_2 atmosphere. The mixture was then heated to 180 °C and kept for 2 h. Finally, the NPs were collected via centrifugation, obtained after washed with ethanol and hexane.

2.1.2. Synthesis of the Pt/C, Pt/CeO_2/C and Pt/Ni–CeO_2/C catalysts

The Pt/C catalyst was synthesized by a microwave-assisted polyol reduction method [9]. Briefly, Vulcan XC-72 carbon powder was mixed with ethylene glycol and isopropanol to form a homogeneous ink, into which H_2PtCl_6 solution was added. Subsequently, after the pH value of the mixture was adjusted to 10 the mixture was subjected to microwave-heating (model-WBFY201, 750 W, 2450 MHz) for 60 s. The Pt/C catalyst was obtained after cooling, washing with deionized water and dried at 80 °C for 3 h. A similar procedure was used for the synthesis of Pt/CeO_2/C and Pt/Ni–CeO_2/C catalysts except that the mixture of Vulcan XC-72 carbon and CeO_2 or Ni–CeO_2 NPs was employed rather than Vulcan XC-72 carbon alone. The loadings of both Pt and CeO_2 (or Ni–CeO_2) for the catalysts are 20 wt%.

2.2. Physical characterization and electrochemical measurement

Transmission electronic microscopy (TEM) and high-resolution TEM (HRTEM) images and energy-dispersive X-ray spectrometry (EDS) were acquired on a FEITECNAI F-30 system. XRD data were carried out on a D/max 2500-γB diffractometer (Cu Kα radiation). X-ray photoelectron spectroscopy (XPS) was performed on a physical electronics PHI model 5700 instrument (Al Kα radiation).

All the electrochemical experiments were conducted in a conventional three-electrode cell at room temperature with Pt foil and Hg/Hg_2SO_4 as the counter and reference electrodes, respectively. Pt/C, Pt/CeO_2/C, or Pt/Ni–CeO_2/C catalysts were suspended in the mixture of isopropyl alcohol and DI water by ultrasonically blending to form a catalyst ink (2.0 mg mL^{-1}). 15 μL of the ink was then pipetted onto the surface of a glassy carbon disk with area of 0.1256 cm^2. After drying, the disk was covered with Nafion solution (0.5%, 5 μL) to serves the working electrode with the same Pt and CeO_2 loading of 47.8 μg cm^{-2}. Cyclic voltammetry (CV) at the scan rate of 50 mV s^{-1} and chronoamperometry (CA) at 0.5 V were conducted in a N_2-saturated 0.5 M H_2SO_4 solution containing 0.5 M ethanol. Unless otherwise specified, all the reported potentials in this Communication are referred to the reversible hydrogen electrode (RHE).

3. Results and discussion

Fig. 1A shows the TEM image of monodispersed Ni–CeO_2 NPs with the average diameter of ~3.7 nm (Fig. S1 in Supporting information) and spherical-like morphology. The electron diffraction pattern (insert of Fig. 1A) indicates the good crystallinity of Ni–CeO_2 NPs. From the HRTEM image of Ni–CeO_2 in Fig. 1B, a polycrystalline structure with two adjacent (111) lattice fringes of 0.317 nm is observed. This value is slightly broader than the

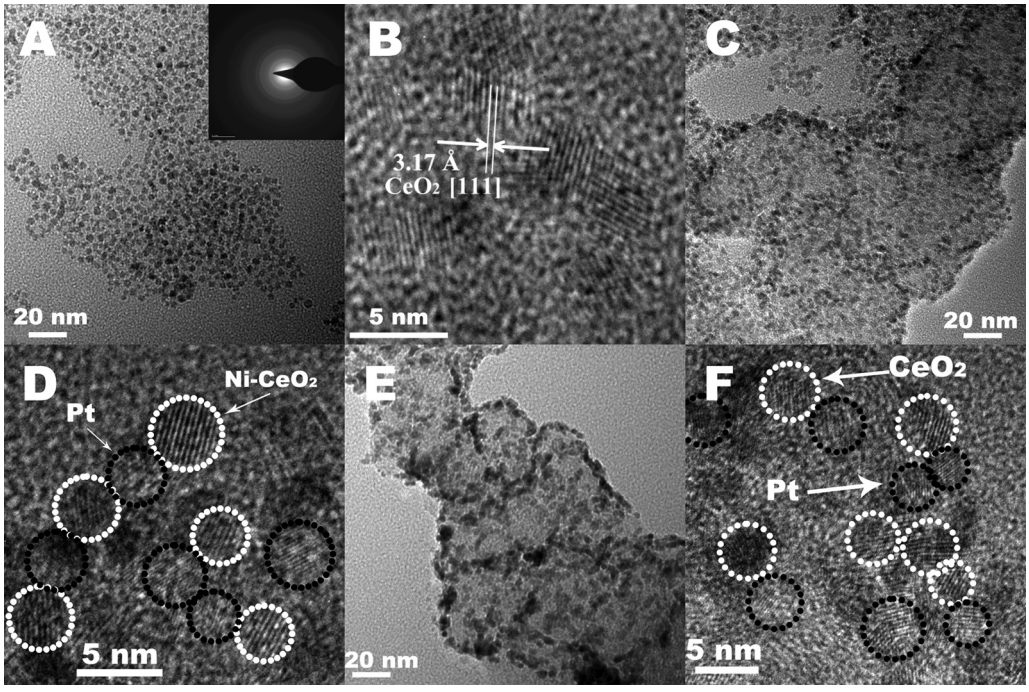

Fig. 1. TEM and HRTEM images of Ni–CeO_2 NPs (A, B), Pt/Ni–CeO_2/C catalyst (C, D) and Pt/CeO_2/C catalyst (E, F). Inset: electron diffraction pattern of Ni–CeO_2 NPs.

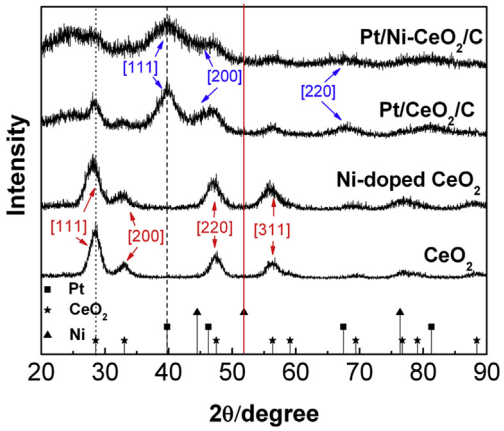

Fig. 2. XRD patterns of CeO_2 NPs, Ni–CeO_2 NPs, Pt/CeO_2/C and Pt/Ni–CeO_2/C.

standard (111) spacing of CeO_2 (0.312 nm) [10], which are ascribed to the Ni doping. It can be clearly seen from the TEM and HRTEM images of Pt/Ni–CeO_2/C catalyst (Fig. 1C and D) that the Pt and Ni–CeO_2 NPs are homogeneously dispersed on the XC-72 carbon support in a narrow size distribution with the average size of Pt NPs approximately 2.8 nm. From the EDS result of the Pt/Ni–CeO_2/C (Fig. S2 in Supporting information), the Ni–CeO_2 NPs contain Ni element of 4.7%, which is roughly in accordance with the original feeding ratio. Due to the similar preparation process, the Pt/CeO_2/C catalyst (Fig. 1E and F) shows a similar morphology with Pt/Ni–CeO_2/C catalyst.

Fig. 2 shows the XRD patterns of CeO_2, Ni–CeO_2, Pt/CeO_2/C and Pt/Ni–CeO_2/C, in which similar diffraction patterns are obtained for CeO_2 and Ni–CeO_2 NPs indexed to the cubic fluorite structure of crystalline CeO_2 (JCPDS Card #34-0394) and consistent with the literature reports [11]. However, the peaks of Ni–CeO_2 NPs are shifted to lower angles, which correspond to a larger *d* spacing due to the Ni doping and consistent with the TEM results. Furthermore, no phase ascribed to Ni compounds can be seen, indicating that all Ni ions have entered into the crystalline lattice of CeO_2 [8]. After the microwave-assisted ethylene glycol process, the resulted products exhibit new diffraction peaks at around 39°, 46° and 68° that are indexed to the (111), (200), and (220) planes of face centered cubic Pt, and the indistinctive diffraction peak at 25° that is indexed to carbon, suggesting that Pt has been successfully loaded on the carbon supports.

Fig. 3A gives CV curves of the Pt/C, Pt/CeO_2/C and Pt/Ni–CeO_2/C catalysts in 0.5 M H_2SO_4 solution, from which the electrochemical surface area (ECSA) is calculated to be 44.38 $m^2\ g^{-1}$, 66.95 $m^2\ g^{-1}$ and 69.06 $m^2\ g^{-1}$, respectively. These ECSA values are bigger than those for Pt/C or Pt/CeO_2/C catalysts in previous reports [12]. The mass activity normalized by Pt loading of Pt/Ni–CeO_2/C towards the ethanol electrooxidation was evaluated by CV in 0.5 M H_2SO_4 and 0.5 M C_2H_5OH solution and compared with the Pt/C and Pt/CeO_2/C catalysts (Fig. 3B). All the voltammetric waves are typical features of the ethanol electrooxidation in acidic media and consistent with the literature reports [13]. During the positive scan, current densities start to increase at ~500 mV due to the oxidation of adsorbed intermediates from ethanol dissociation, reach the maximum for ethanol electrooxidation at ~900 mV, and then decrease as a result of the adsorption of water or anions. During the negative scan, the peak for ethanol electrooxidation is observed at ~700 mV. The forward current densities at 0.5 V, which is close to the practical anode potential in DEFCs, are used to evaluate the catalytic activities of these catalysts towards the ethanol electrooxidation. The current density for Pt/Ni–CeO_2/C catalyst is 199.3 mA mg^{-1}, which is 1.56 and 3.76 times higher than that for

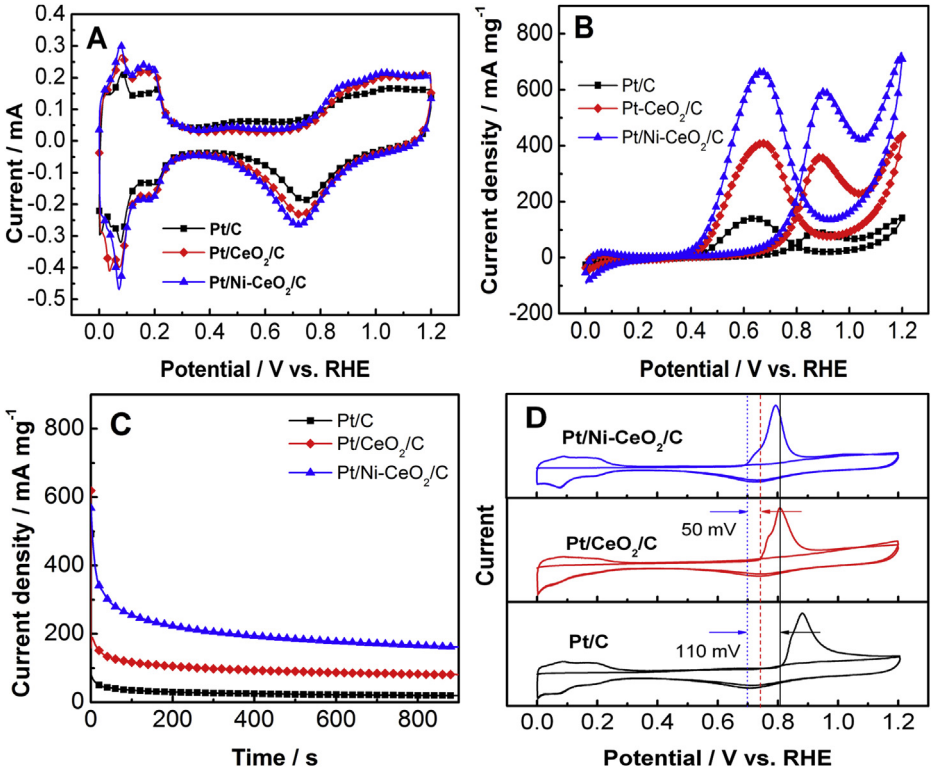

Fig. 3. CV curves (A) of Pt/C, Pt/CeO_2/C and Pt/Ni–CeO_2/C catalysts in 0.5 M H_2SO_4 solution, CV (B) and CA at 0.5 V (C) curves of Pt/C, Pt/CeO_2/C and Pt/Ni–CeO_2/C catalysts in 0.5 M H_2SO_4 + 0.5 M C_2H_5OH solution, and CO stripping curves (D) of Pt/C, Pt/CeO_2/C and Pt/Ni–CeO_2/C catalysts in N_2-saturated 0.5 M H_2SO_4 solution.

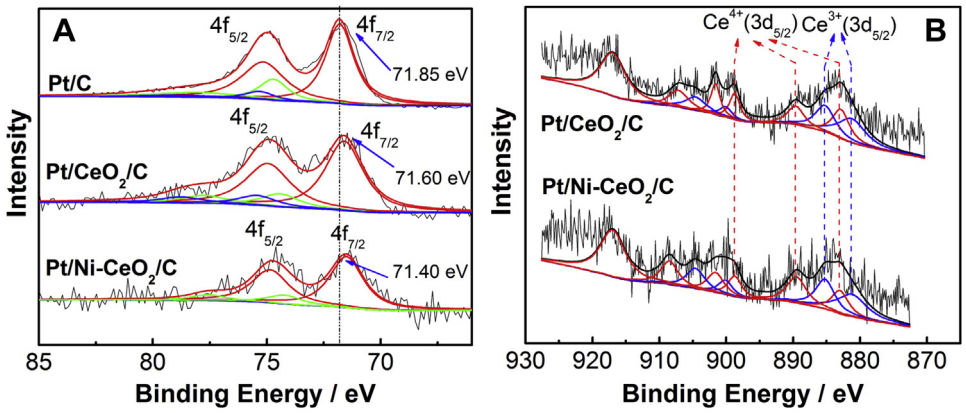

Fig. 4. (A) Pt (4f) XPS spectra of Pt/C, Pt/CeO_2/C and Pt/Ni–CeO_2/C, (B) Ce (3d) XPS spectra of Pt/CeO_2/C and Pt/Ni–CeO_2/C.

Pt/CeO_2/C (127.7 mA mg^{-1}) and Pt/C (53.0 mA mg^{-1}) catalysts, respectively. Also, this current density is even higher than that of the benchmark PtRu/C (ca. 97.2 mA mg^{-1}) and PtSn/C (ca. 108.7 mA mg^{-1}) catalysts (Fig. S3 in Supporting information), which were synthesized by a microwave-assisted polyol reduction method (see Supporting information for details). The mass activity of our Pt/Ni–CeO_2/C catalyst is among the highest values reported [14–16] and consistent with the fuel cell performance (Fig. S4 in Supporting information). The specific activity normalized by ECSA confirms the high activity of the Pt/Ni–CeO_2/C catalyst (Fig. S5 in Supporting information). Moreover, the Pt/Ni–CeO_2/C catalyst exhibits a current density that is 1.99 and 8.30 times higher than Pt/CeO_2/C and Pt/C catalysts even after 900 s of CA test (Fig. 3C). Actually, the Pt/Ni–CeO_2/C catalyst also has significantly high activity for the methanol oxidation reaction as revealed by CV (Fig. S6 in Supporting information) and CA (Fig. S7 in Supporting information) curves. All these results clearly demonstrate that the catalytic activity and tolerance to poisoning species of the Pt/Ni–CeO_2/C enhanced by the Ni–CeO_2 NPs.

According to the previous reports [13,14,17], the ethanol electrooxidation on Pt-based catalysts involves the successive dehydrogenation of ethanol, leading to formation of poisoning intermediates, such as acetaldehyde for partial oxidation and CO for total oxidation of ethanol. In order to verify the high tolerance of Pt/Ni–CeO_2/C to poisoning species, CO stripping voltammograms were used to probe the oxidation potential of CO adsorbed on catalyst surfaces. As shown in Fig. 3D, the Pt/C catalyst has an onset potential of CO oxidation at 0.80 V, whereas the as-prepared Pt/CeO_2/C and Pt/Ni–CeO_2/C catalysts show lower onset potentials at 0.74 V and 0.69 V, respectively. This result indicates that CeO_2 can facilitate the CO oxidation, which is probably due to the oxygen-species facilely released from CeO_2 [18]. Moreover, after Ni doping, Ni–CeO_2 could release more oxygen-species to promote CO oxidation, even at low potentials, which is good for the ethanol electrooxidation [19]. In addition to CO, the electrooxidation of acetaldehyde was also evaluated (Fig. S8 in Supporting information). The Pt/Ni–CeO_2/C exhibits higher activity to the acetaldehyde oxidation than Pt/C and Pt/CeO_2/C catalysts, which is similar to the CO stripping voltammograms and demonstrates the high tolerance of Pt/Ni–CeO_2/C to various poisoning species.

XPS was performed to analyze composition and chemical state of the Pt/C, Pt/CeO_2/C and Pt/Ni–CeO_2/C catalysts, from which Ni–CeO_2 contains about 5.5% of Ni element, roughly in accordance with the theoretical feeding ratio. Fig. 4A presents the detailed Pt (4f) XPS spectra for Pt/C, Pt/CeO_2/C and Pt/Ni–CeO_2/C. Pt $4f_{7/2}$ and $4f_{5/2}$ peaks of Pt/Ni–CeO_2/C show 0.20 eV and 0.45 eV of negative shift compared with Pt/CeO_2/C and Pt/C, respectively. The shift indicates that there is enhanced electronic interaction between Pt and Ni–CeO_2, and the *d*-band center of Pt is lowered due to the electron transfer between Pt and Ni–CeO_2. This electronic effect is beneficial to the removal of the poisoning intermediates and thus the enhancement of activity [20,21]. Fig. 4B shows the detailed Ce (3d) XPS spectra for Pt/CeO_2/C and Pt/Ni–CeO_2/C. From the deconvoluted results of the previous report [22], the Ce^{3+} content in Pt/CeO_2/C and Pt/Ni–CeO_2/C is 37.30% and 45.53% respectively, indicating that the oxygen-vacancy formation energy of Ni–CeO_2 is decreased by Ni doping. This is mostly due to the structure distortion and electronic modification of CeO_2 as revealed in previous studies [23,24]. Therefore, Pt/Ni–CeO_2/C catalyst has easier oxygen releasing capability and thus higher oxidizing rate of the poisoning intermediates, undoubtedly leading to better activity towards the ethanol oxidation reaction.

4. Conclusion

Monodispersed Ni–CeO_2 NPs with the size of ~4 nm and spherical-like morphology were first synthesized by a facile thermal decomposition method, which can considerably promote the activity and stability of the conventional Pt/C catalyst towards the ethanol oxidation reaction in acidic media. It suggests that the Ni-doping alters the electronic structure of CeO_2, leading to high oxygen-releasing ability and improved interaction with Pt, which are beneficial to the removal of poisoning intermediates and the enhancement of catalytic properties for Pt/Ni–CeO_2/C catalyst. Metal doped oxides can not only be used for fuel cell catalysts but also be potentially extended to other catalytic fields.

Acknowledgments

This work is funded by National Natural Science Foundation of China under Contracts 20706010 and 21376057, and the NSRI Foundation in the Harbin Institute of Technology.

Appendix A. Supplementary data

Supplementary data related to this article can be found at http://dx.doi.org/10.1016/j.jpowsour.2014.04.062.

References

[1] F. Vigier, C. Coutanceau, A. Perrard, E.M. Belgsir, C. Lamy, J. Appl. Electrochem. 34 (2004) 439–446.
[2] Y. Shao, G. Yin, Y. Gao, J. Power Sources 171 (2007) 558–566.
[3] C. Xu, P.K. Shen, Y. Liu, J. Power Sources 164 (2007) 527–531.

[4] C. Xu, P.K. Shen, X. Ji, R. Zeng, Y. Liu, Electrochem. Commun. 7 (2005) 1305–1308.
[5] C.Y. Du, M. Chen, X.Y. Cao, G.P. Yin, P.F. Shi, Electrochem. Commun. 11 (2009) 496–498.
[6] C. Zhou, H. Wang, F. Peng, J. Liang, H. Yu, J. Yang, Langmuir 25 (2009) 7711–7717.
[7] K.W. Park, J.H. Choi, K.S. Ahn, Y.E. Sung, J. Phys. Chem. B 108 (2004) 5989–5994.
[8] K.W. Park, K.S. Seol, Electrochem. Commun. 9 (2007) 2256–2260.
[9] M. Chen, C.Y. Du, J. Zhang, P.P. Wang, T. Zhu, J. Power Sources 196 (2011) 620–626.
[10] C. Sun, H. Li, H. Zhang, Z. Wang, L. Chen, Nanotechnology 16 (2005) 1454–1463.
[11] S.S. Lee, H.G. Zhu, E.Q. Contreras, A. Prakash, H.L. Puppala, V.L. Colvin, Chem. Mater. 24 (2011) 424–432.
[12] C.W. Xu, P.K. Shen, Chem. Commun. 19 (2004) 2238–2239.
[13] J. Seweryn, A. Lewera, Appl. Catal. B Environ. 144 (2014) 129–134.
[14] Z.L. Liu, X.Y. Ling, X.D. Su, J.Y. Lee, L.M. Gan, J. Power Sources 149 (2005) 1–7.
[15] A.O. Neto, M. Linardi, D.M. Anjos, G.T. Filho, E.V. Spinace, J. Appl. Electrochem. 39 (2009) 1153–1156.
[16] A. Brouzgou, S.Q. Song, P. Tsiakaras, Appl. Catal. B Environ. 127 (2012) 371–388.
[17] Y. Wang, S.Q. Song, G. Andreadis, H. Liu, P. Tsiakaras, J. Power Sources 196 (2011) 4980–4986.
[18] H. Yuan, D. Guo, X. Li, L. Yuan, W. Zhu, L. Chen, X. Qiu, Fuel Cells 9 (2009) 121–127.
[19] A.B. Kehoe, D.O. Scanlon, G.W. Watson, Chem. Mater. 23 (2011) 4464–4468.
[20] B. Hammer, Y. Morikawa, J.K. Nørskov, Phys. Rev. Lett. 76 (1996) 2141–2144.
[21] Y. Morikawa, J.J. Mortensen, B. Hammer, J.K. Nørskov, Surf. Sci. 386 (1997) 67–72.
[22] F. Lin, D. Hoang, C.K. Tsung, W. Huang, S. Lo, J. Wood, H. Wang, J. Tang, P. Yang, Nano Res. 4 (2011) 61–71.
[23] Y.H. Tang, H. Zhang, L.X. Cui, C.Y. Ouyang, S.Q. Shi, W.H. Tang, H. Li, J.S. Lee, L.Q. Chen, Phys. Rev. B 82 (2010) 125104–125113.
[24] K.H. You, H. Graeme, J. Phys. Chem. Lett. 16 (2012) 2194–2199.